SUPPLEMENTARY INFORMATION

Combined spectroscopic and computational study for optimising catalyst design in hydrocarbon transformations

M. E. Potter[a]*, J. J. M. Le Brocq[a], A. E. Oakley[a], H. Cavaye [b], B. D. Vandegehuchte[c] and R. Raja[a]

a) School of Chemistry, University of Southampton, Southampton, HANTS, SO17 1BJ, UK.

b) ISIS Neutron and Muon Source, STFC Rutherford Appleton Laboratory, Harwell Campus, Didcot, Oxon, OX11 0QX, UK.

c) TotalEnergies OneTech Belgium, Zone Industrielle Feluy C, B-7181 Seneffe, Belgium.

* MEP = M.E.Potter@soton.ac.uk

Table of contents

Experimental

Chemicals: 99.9% purity n-Butane was used, as received from BOC gases. The MOR used was a commercial Zeolyst sample (CBV 21A), in the ammonium form, with a SiO_2/Al_2O_3 mole ratio of 20. The sample was calcined at 500 °C for 16 hours in air to obtain the protonated form, prior to any measurements.

Powder X-ray diffraction: Powder X-ray diffraction was performed on a Bruker D2 Phaser diffractometer with Cu Kα1 radiation. Patterns were run over a 2θ range of 5–40 ° with a scan speed of 3 °/min and an increment of 0.01 °.

Nitrogen physisorption: Nitrogen physisorption were performed at 77 K, on a sample dried under 20 mTorr of vacuum at 120 °C overnight. Analysis was performed on a Micromeritics Gemini 2375 surface area analyser. Surface area was calculated using the BET model,[1] and the pore width distributions was determined using the BJH method.[2]

ICP: Si and Al quantities were obtained through the commercial MEDAC ICP system.

Solid state NMR: Solid state NMR measurements were performed by packing samples into 3.2 mm rotors. Acquisitions were carried out at a spinning rate of 20 kHz in double resonance mode, using a Bruker Avance Neo Spectrometer with a 9.4 T field, in air. The sample ^{1}H, ^{27}Al, T_1 was assessed using a saturation recovery pulse technique, which was used for the respective direct acquisitions, and the ^{1}H-^{29}Si cross-polarisation.

SEM: Scanning electron microscopy (SEM) images were acquired at the Southampton Biomedical Imaging Unit, using an FEI Quanta 250 FEG scanning electron microscope. Samples were sputter coated with platinum prior to imaging.

n-Butane isomerisation: Catalytic butane isomerisation measurements were performed using a fixed bed reactor, containing 0.3 g of calcined MOR, pelletised and sieved between 300 – 500 µm. The sample was dried at 400 °C for 1 hour under a 80 mL/min flow of nitrogen in the reactor prior to the reaction. After this the gas flow was changed to 5 mL/min of 10 % n-butane in nitrogen, at 300 °C under atmospheric pressure. Samples taken every 15 minutes using an online Perkin Elmer Arnel 4035 gas chromatogram, with a FID with an Alumina Sulfate PLOT column, 50 m x 0.53 mm.

INS data collection: INS measurements were performed on the TOSCA beamline at the ISIS Neutron and Muon Source, Didcot, under the experimental DOI: 10.5286/ISIS.E.RB1920057.[3] 10 g of calcined MOR was dried at 200 °C under vacuum for 8 hours prior to measurement, *in situ* in an Inconel cell. The INS spectrum of the evacuated system was then collected for 16 hours at 20 K. The system was then heated to room temperature, when the ISIS gas handling rig was used to fill 10% of the zeolite pore volume with butane, corresponding to a theoretical 1:4.4 molar ratio of butane to acid sites. The quantity of butane introduced was purposefully limited so that the system exclusively contained butane, within the MOR pore, interacting with the acid sites. The INS data of this system was collected for 16 hours, at 20 K. Analogous data were collected for the empty Inconel cell for data subtraction. The spectra of pure butane and the corresponding empty gas-cell were collected at 20 K over 2 hours. All the data were reduced and analysed using the Mantid program.[4] All data presented have had the background and empty can subtracted.

DFT Calculations: All calculations used the CRYSTAL17 code.[5] For all calculations the Grimmes D3 dispersion correction was used, with the 3-body Axilrod-Teller-Muto term.[6, 7] Calculations were performed using the default extra-large grid size with 75 radial points and 974 angular points, in regions of relevant bonding, with each atomic grid split into five shells of different angular grids. The

B3LYP hybrid functional,[8-11] along with the periodic Gaussian basis sets from Bredow *et al* were used.[12, 13] Systems were calculated using a shrinking factor of 2 for both reciprocal space and the Gilat net. The truncation criteria for the bielectronic integrals were set to 10^{-8} for the overlap and penetration thresholds for the coulomb integrals and also the overlap threshold for the HF-exchange integrals. The convergence criteria for the pseudo overlap in the HF series were set to 10^{-8} and 10^{-16} as necessary. The total energy convergence criteria were set to 10^{-11} au, while the thresholds for the maximum and RMS gradient were 0.00045 and 0.0003 au respectively. Similarly, the maximum and RMS displacement thresholds were 0.0018 and 0.0012 respectively. To optimise the empty MOR system the unit cell parameters and atomic positions were unconstrained. For systems with butane within the MOR system, the cell parameters and cell volumes were fixed, and the optimisation was performing in internal redundant coordinates. Constrained optimisations to calculate the butane rotation energy profile were performed by freezing the C-C-C-C dihedral angle, allowing a maximum trust radius of 0.1 angstroms to prevent the system deviating from the frozen parameters. DFT frequency calculations were performed using the same computational parameters using pre-optimised geometries. The CRYSTAL frequency output files were converted to calculated INS spectra using the Abins feature in Mantid, using 2nd order quantum events.[14]

Physicochemical and textural data

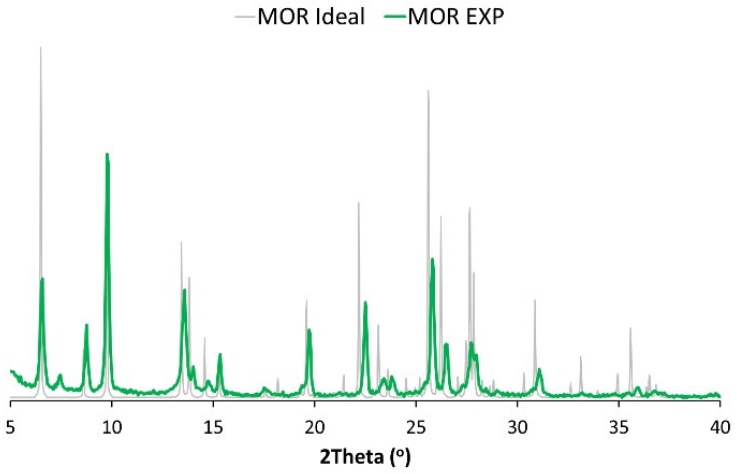

Figure S1: Powder XRD patterns of commercial mordenite, comparing the ideal (MOR ideal) and experimental (MOR EXP) data.

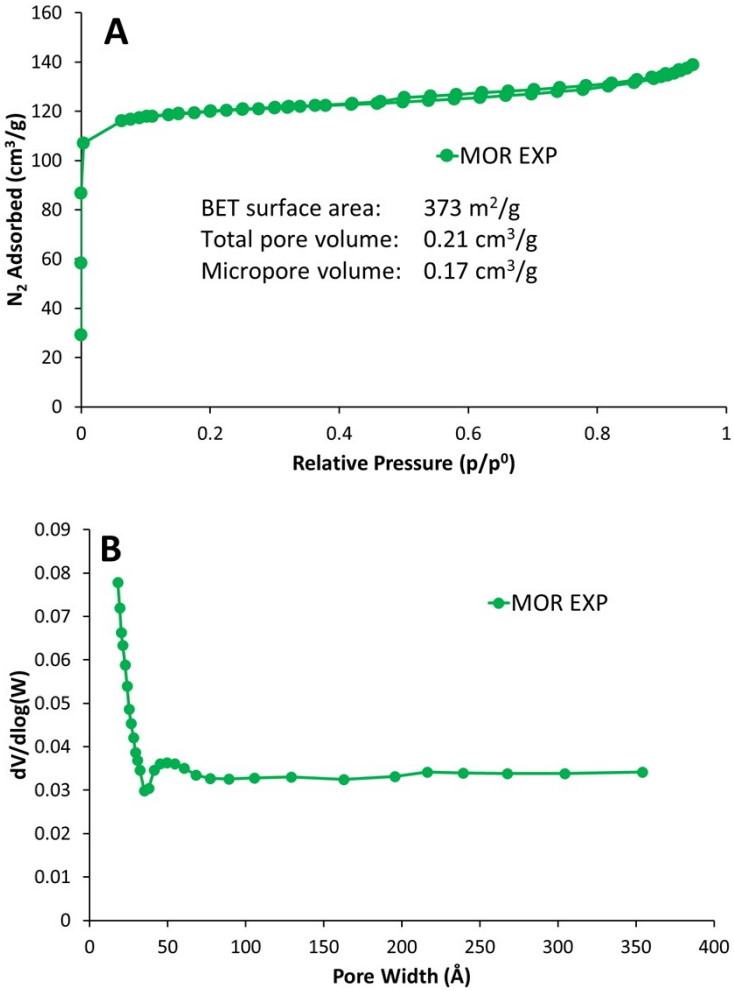

Figure S2: Experimental nitrogen physisorption data of commercial mordenite sample showing the isotherms (A) and BJH pore distribution (B).

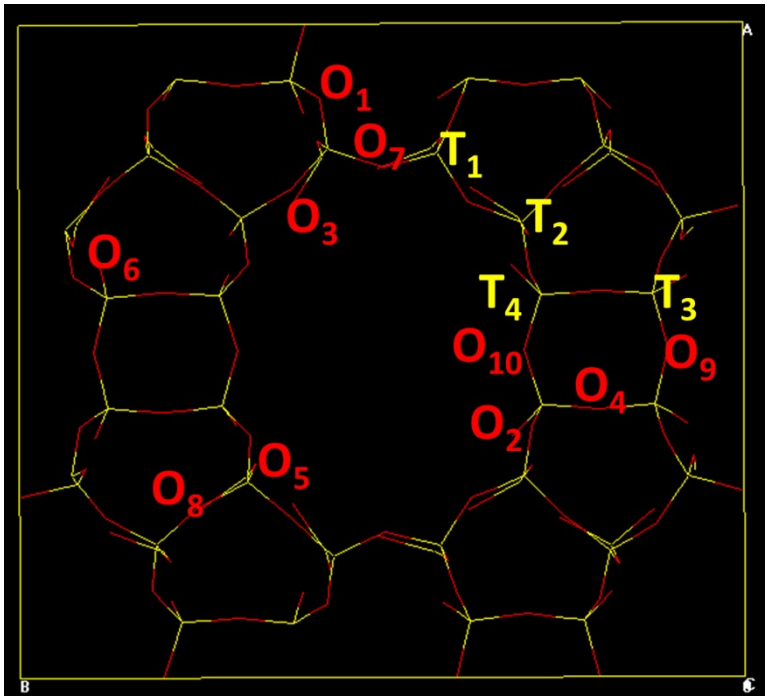

Figure S3: Showing the distinct crystallographic T sites and oxygen atoms in the mordenite unit cell.

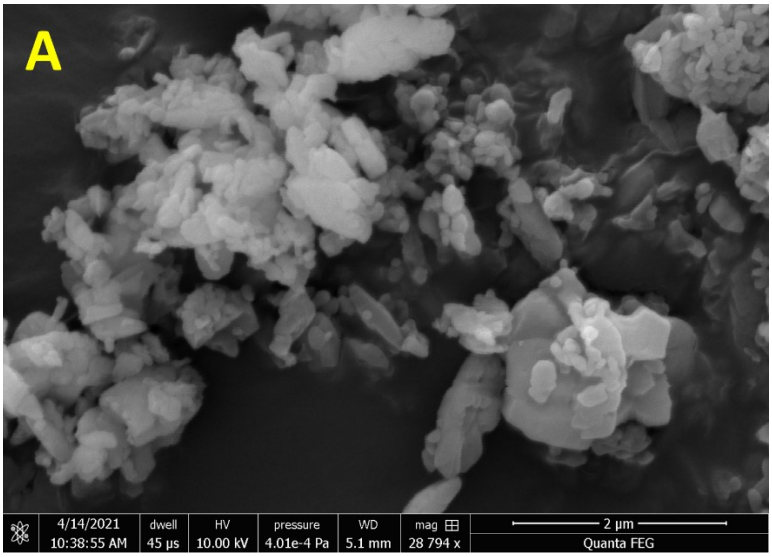

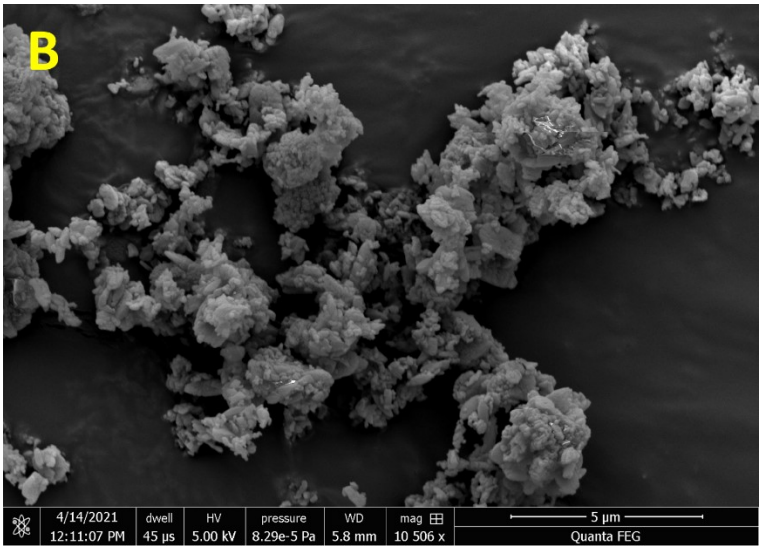

Figure S4: Scanning electron microscopy (SEM) images of the commercial mordenite system.

Solid state NMR findings

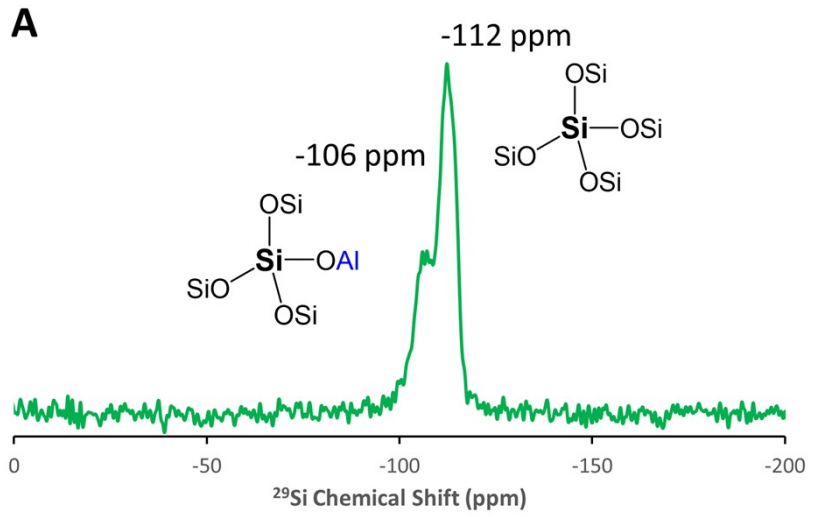

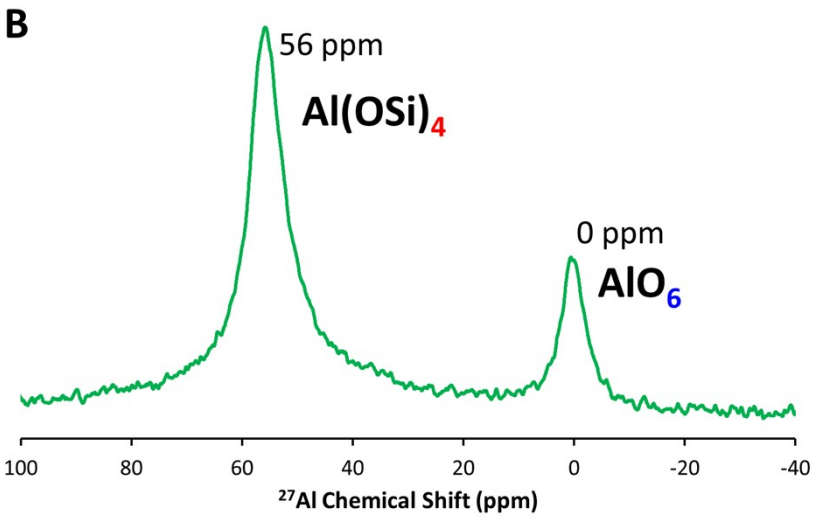

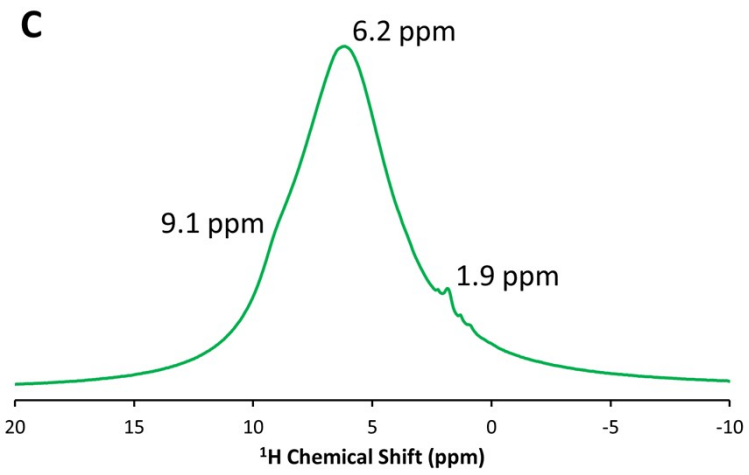

Figure S5: Solid state NMR findings of the commercial mordenite sample focussing on the ^{29}Si (A), ^{27}Al (B) and ^{1}H (C) nuclei.

n-Butane isomerisation catalysis results

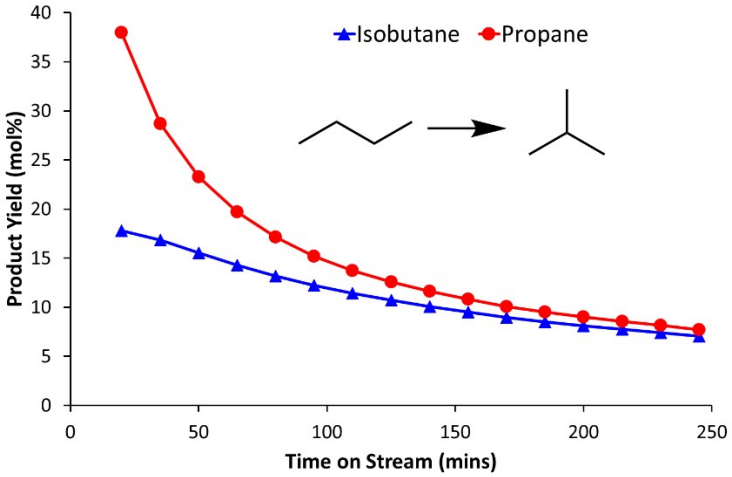

Figure S6: Showing the activity of the commercial mordenite sample for n-butane isomerisation. Reaction conditions: 0.3 g of catalyst, 300 °C, 5 mL/min of 10 % n-butane in nitrogen.

Experimental INS spectra of MOR Zeolite

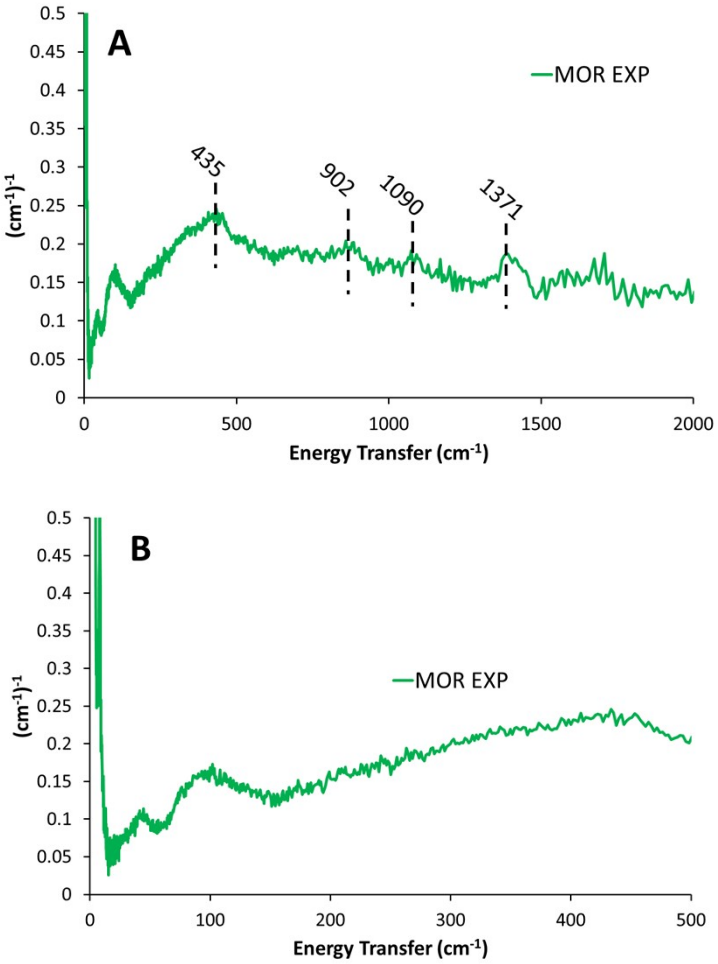

Figure S7: The experimental INS spectrum of bare undoped mordenite at less than 2000 cm^{-1} (A) and focussed on the 0 – 500 cm^{-1} region (B).

Experimental and DFT calculated INS spectra of pure n-butane

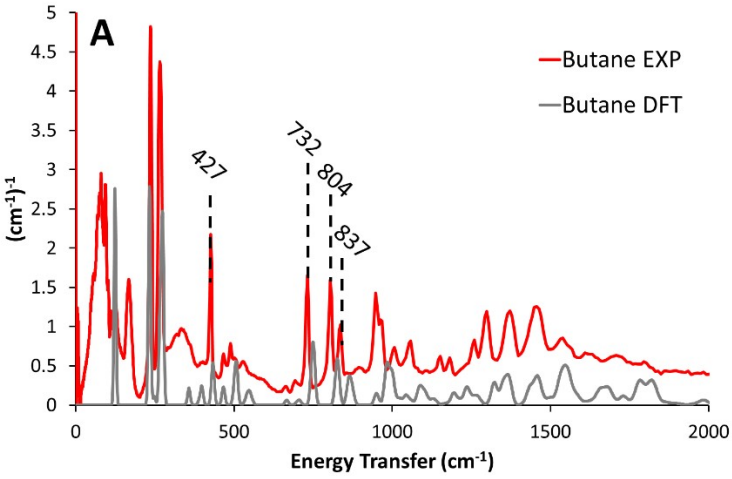

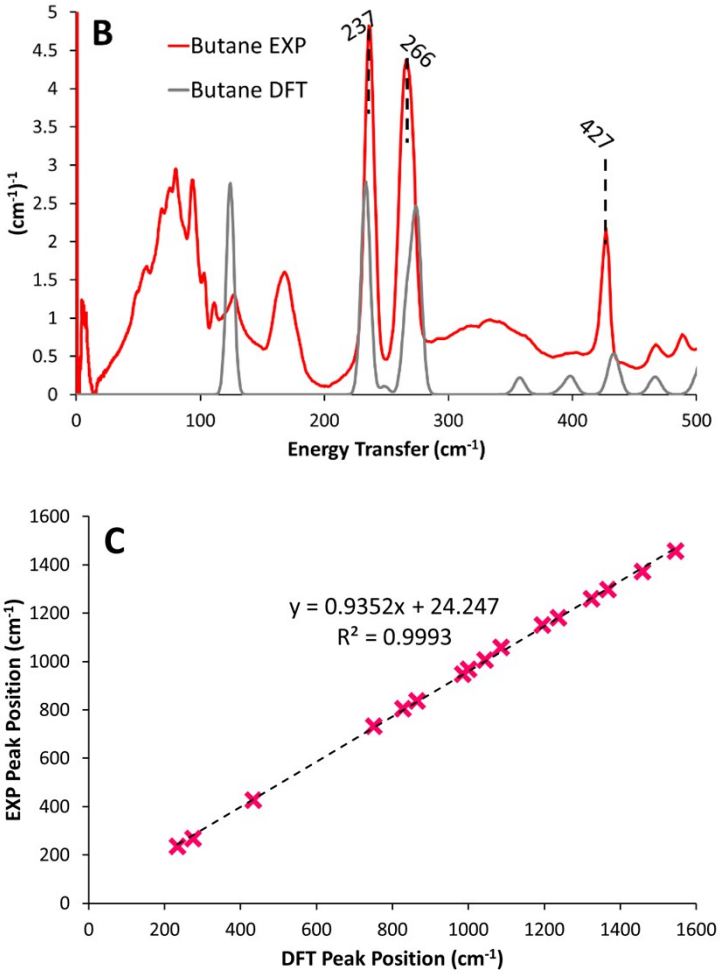

Figure S8: Comparing the theoretical (Butane DFT) and experimental (Butane EXP) INS spectra of n-butane over the extended energy transfer range (A; < 2000 cm^{-1}), and correlating the peak positions (B).

Experimental INS spectra of pure n-butane and n-butane in MOR zeolite

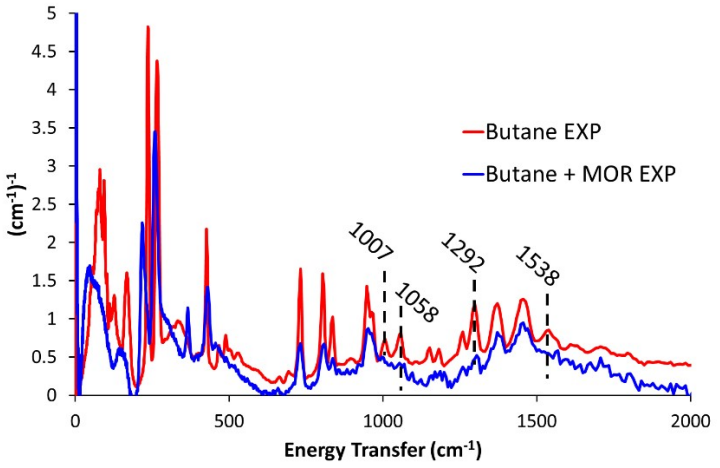

Figure S9: The difference in the experimental INS spectra on encapsulating butane into commercial mordenite (Butane + MOR EXP), compared to pure n-butane (Butane EXP), for < 2000 cm^{-1}.

DFT calculated INS spectra of bare siliceous mordenite

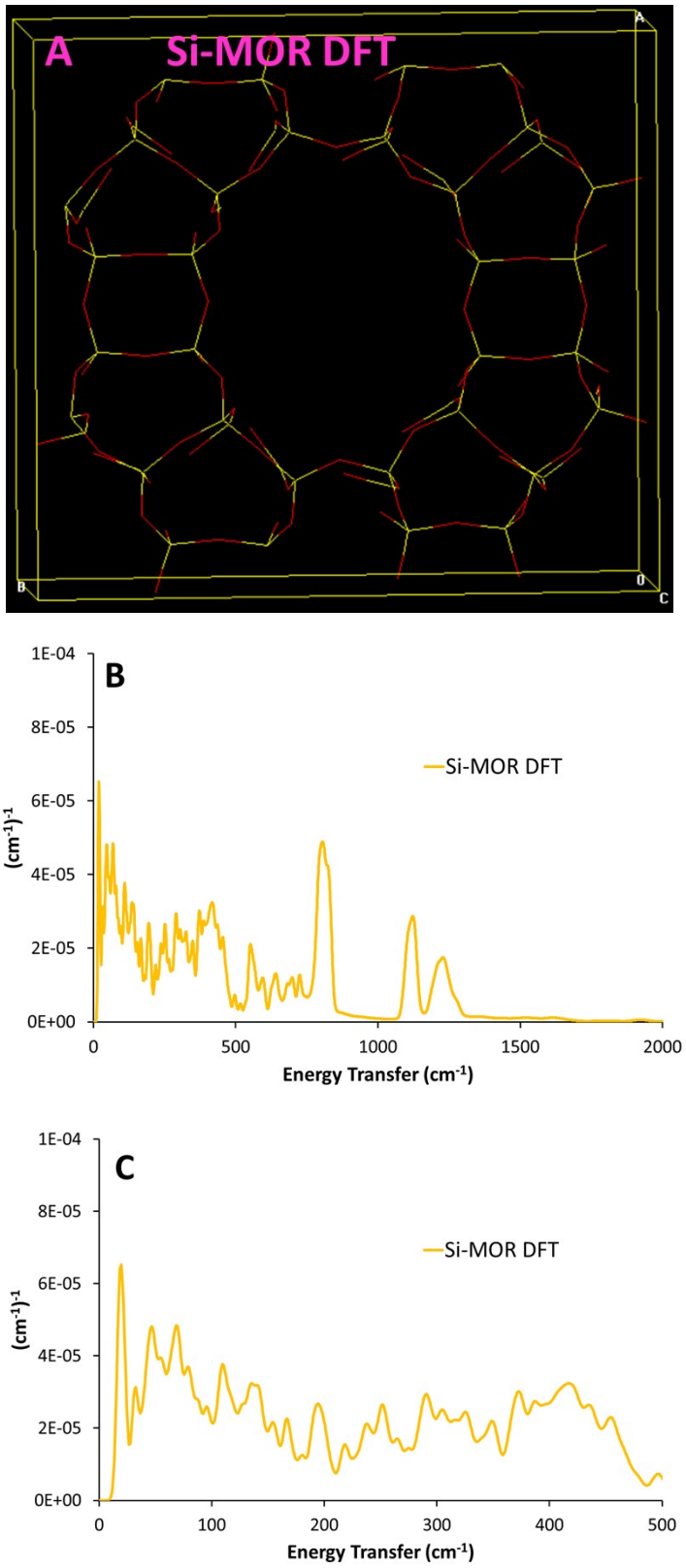

Figure S10: Showing the DFT-optimised geometry of purely siliceous mordenite, Si-MOR DFT, (A) and the corresponding calculated INS spectra over an extended energy range (< 2000 cm^{-1}; B) and a focussed energy range (< 500 cm^{-1}; C).

DFT calculated INS spectra of butane within siliceous mordenite

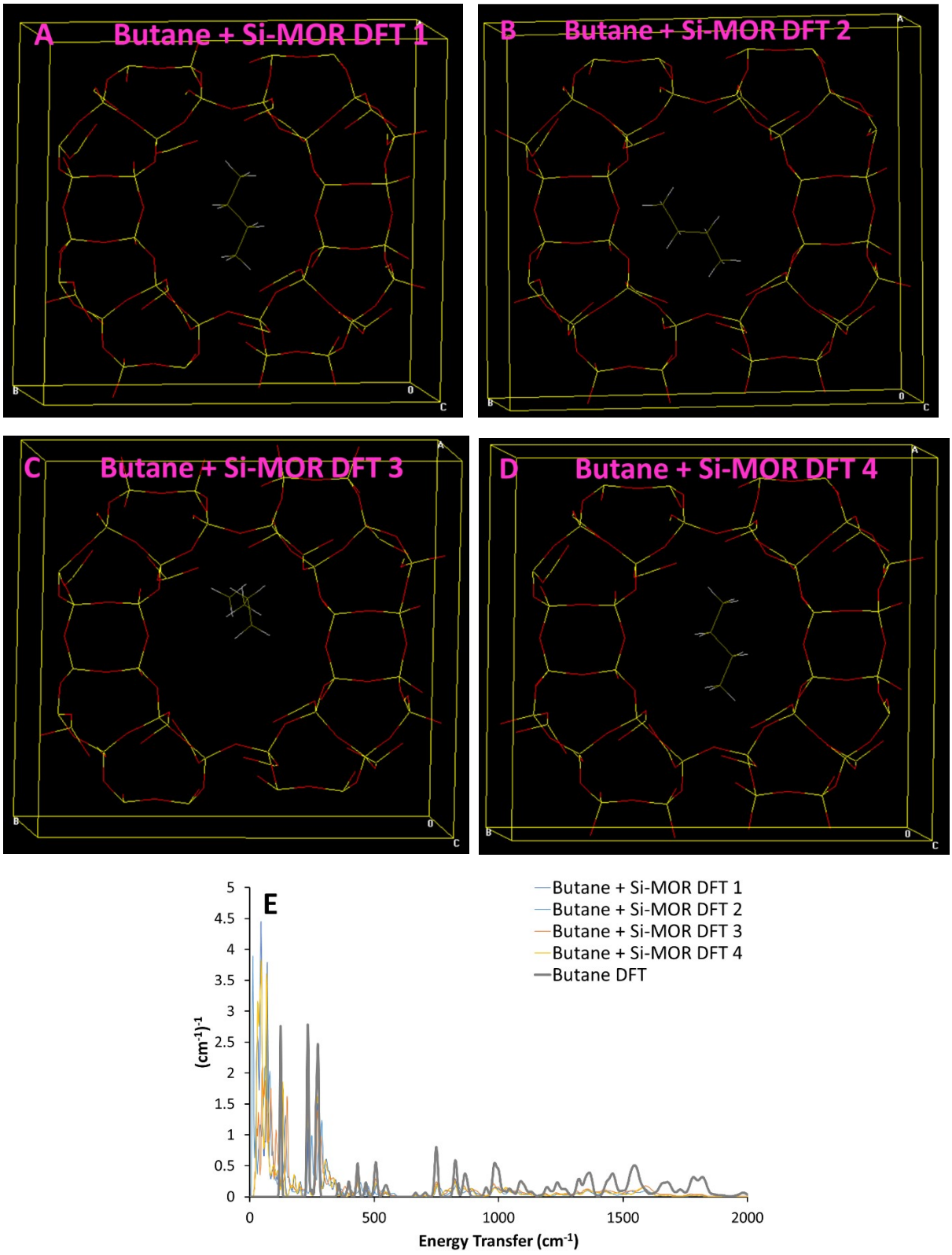

Figure S11: The DFT optimised geometries of n-butane in the siliceous neutral mordenite pore (A-D) and the calculated INS spectra, compared to pure n-butane (E).

Table S1: Comparing the binding energies of n-butane in different geometries within neutral siliceous mordenite, as calculated from Figure S11.

System	Initial Butane Orientation	Binding Energy (kJ/mol)
('Unconfined' Butane) + (Empty Si-MOR)	N/A	0
Butane + Si-MOR DFT 1	Along A	-90
Butane + Si-MOR DFT 2	Along B	-90
Butane + Si-MOR DFT 3	Along C	-96
Butane + Si-MOR DFT 4	Along A (against pore wall)	-90

DFT calculated INS spectra of Al-substituted mordenite

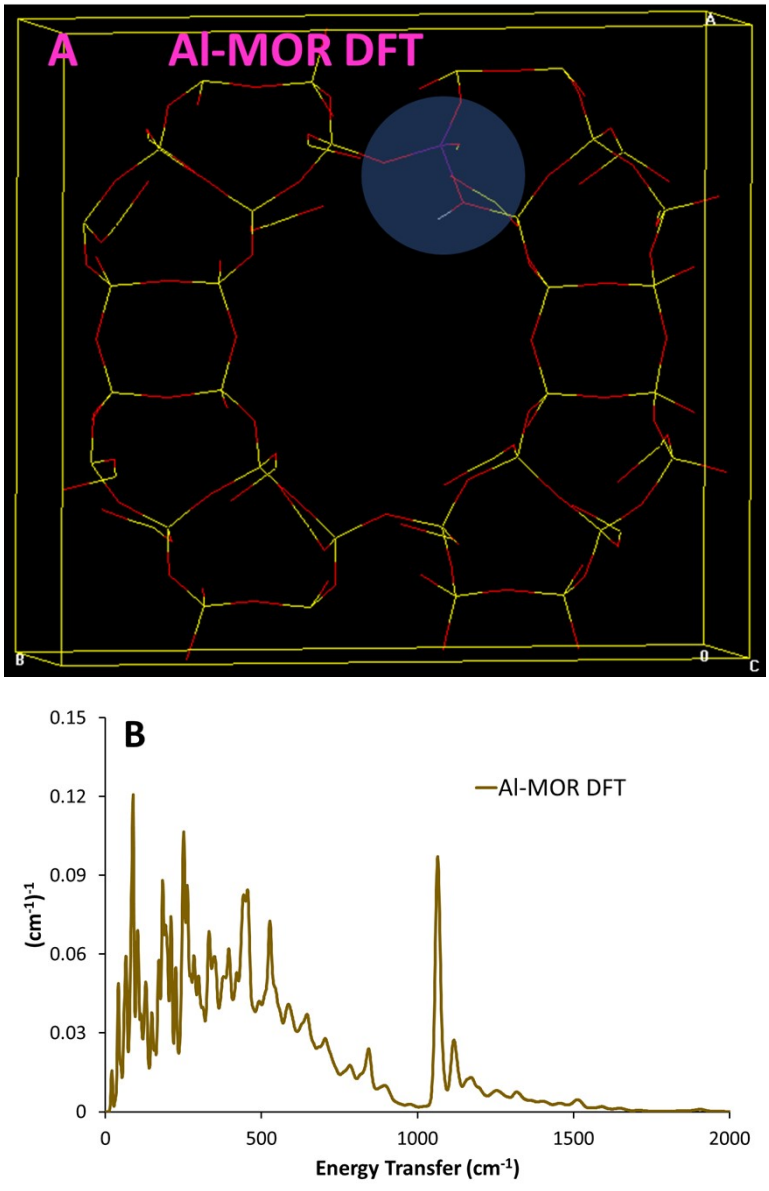

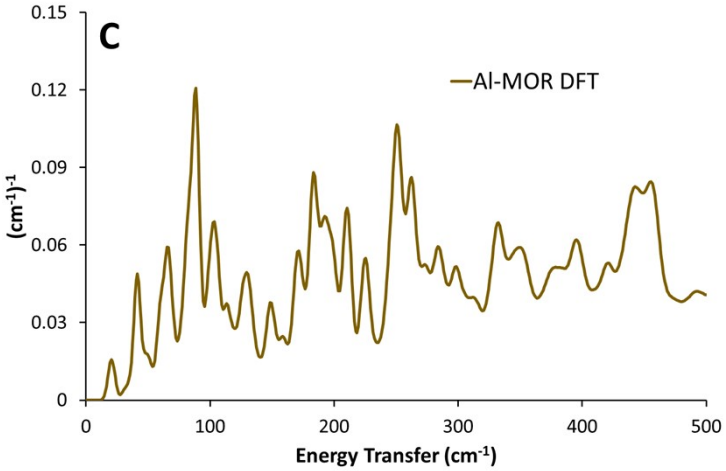

Figure S12: Showing the DFT-optimised geometry of Al-substituted acidic mordenite, Al-MOR DFT, (A) and the corresponding calculated INS spectra over an extended energy range (< 2000 cm^{-1}; B) and a focussed energy range (< 500 cm^{-1}; C).

DFT calculated INS spectra of butane within acidic Al-substituted mordenite

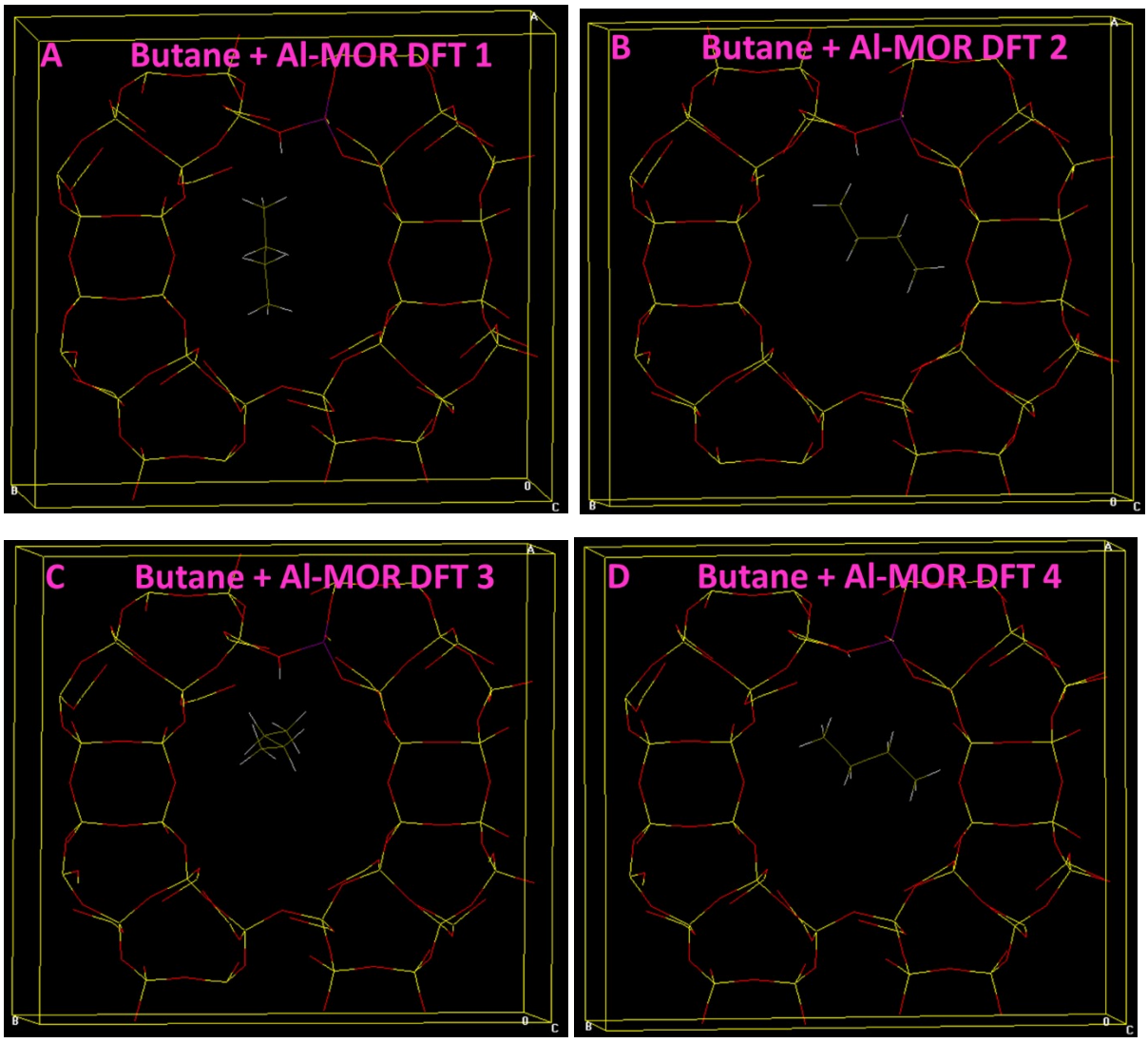

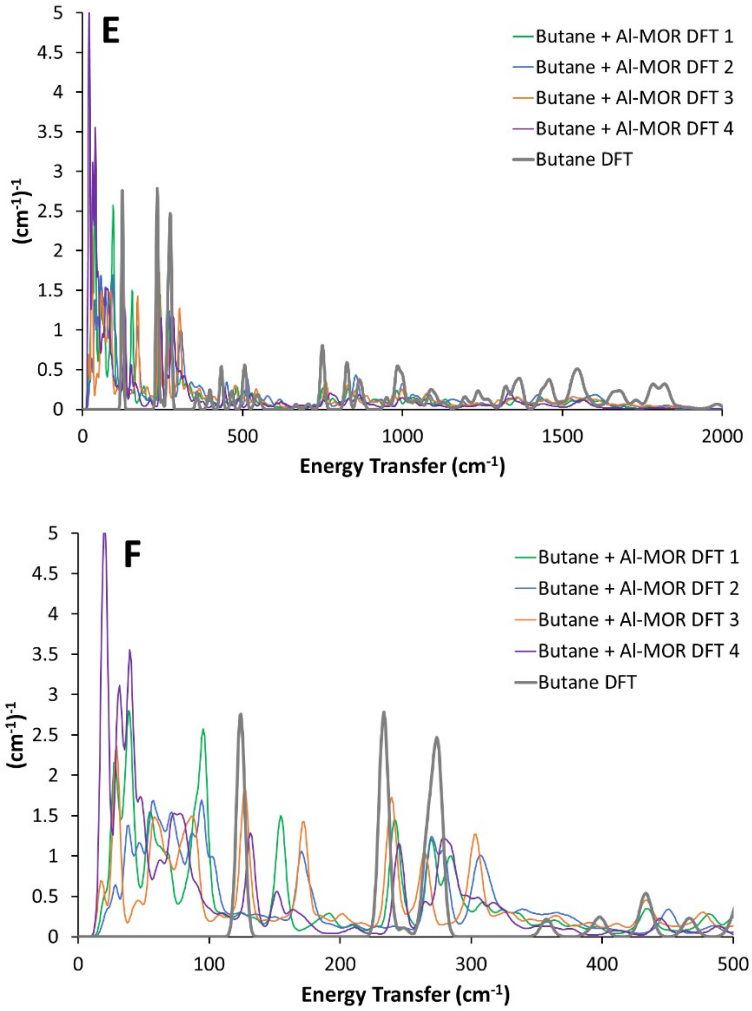

Figure S13: The DFT optimised geometries of n-butane in the acidic Al-substituted mordenite pore (A-D) and the calculated INS spectra, compared to pure n-butane (E,F).

Table S2: Comparing the binding energies of n-butane in different geometries within acidic Al-substituted mordenite, as calculated from Figure S13.

System	Initial Butane Orientation	Binding Energy (kJ/mol)
('Unconfined' Butane) + (Empty Al-MOR)	N/A	0
Butane + Al-MOR DFT 1	Along A	-89
Butane + Al-MOR DFT 2	Along B	-91
Butane + Al-MOR DFT 3	Along C	-87
Butane + Al-MOR DFT 4	Along B (against pore wall)	-86

DFT Parameter Study

To assess the accuracy of our system we compared our calculated binding energies for B3LYP+D3 with PBE+D3 and PBE with no dispersion corrections for both neutral (Si-MOR) and acidic (Al-MOR) mordenite species (Table S1).

Table S3: DFT Parameter study comparing functionals and dispersion corrections

System	Functional	Dispersion Correction	n-Butane Binding Energy (kJ/mol)
Si-MOR	B3LYP	D3	-90.9
Al-MOR	B3LYP	D3	-91.4
Si-MOR	PBE	D3	-87.3
Al-MOR	PBE	D3	-84.0
Si-MOR	PBE	N/A	-25.6
Al-MOR	PBE	N/A	-30.2

Here we show that the calculated bindings energies using both the PBE and B3LYP functionals are in excellent agreement with one another, though clearly the functional choice has far less of an influence than the choice of dispersion correction. In this work we have selected the D3 dispersion correction, as this has been shown to be more accurate than the previous D2 correction.[6, 7] Previous work alkane absorption in zeolites, generally show lower binding energies than those calculated here, however these are either based on the previous D2 Grimme correction, or focus on alternative zeolite host,[15] such as ZSM-5.[16] Previous work on butane isomerisation has shown the 1D mordenite pore is more restrictive than 3D ZSM-5 pore,[17] thus, explaining the greater dispersion energy, and higher binding energy for butane seen in this work. The comparison with the PBE functional (Table S3) also confirms the limited influence of the proton site in mordenite with regards to n-butane binding.

Different n-butane conformers

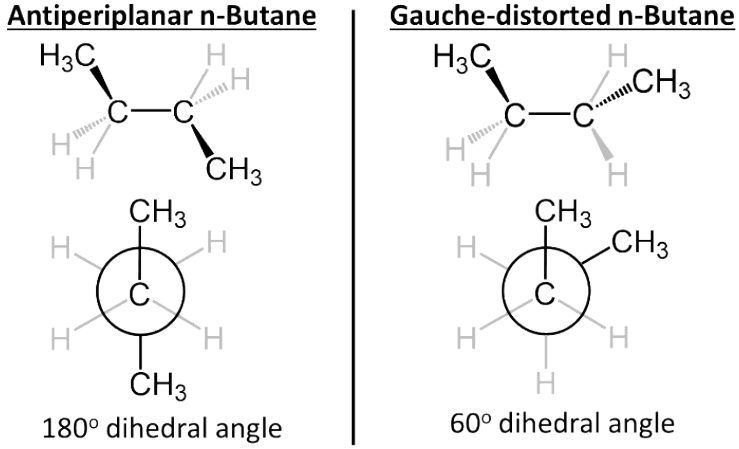

Figure S14: Comparing the geometries of the difference n-butane conformers.

DFT calculated INS spectra of different n-butane conformers

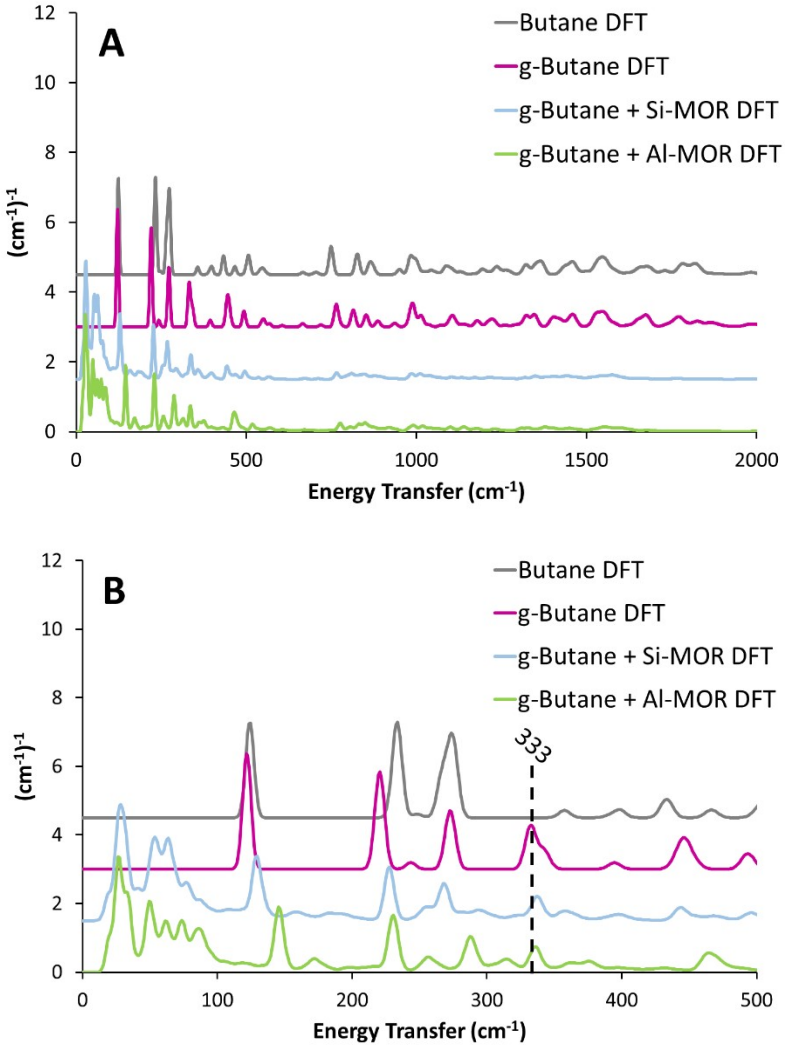

Figure S15: The calculated INS spectra of unconfined n-butane (Butane DFT), unconfined gauche distorted butane (g-Butane DFT) and confined gauche distorted butane within siliceous (Si-MOR) and acidic (Al-MOR) mordenite pores over a wide energy range (< 2000 cm^{-1}, A) and a lower energy range (< 500 cm^{-1}, B) of n-butane. Spectra are artificially shifted by 1.5 $(cm^{-1})^{-1}$ for ease of reading.

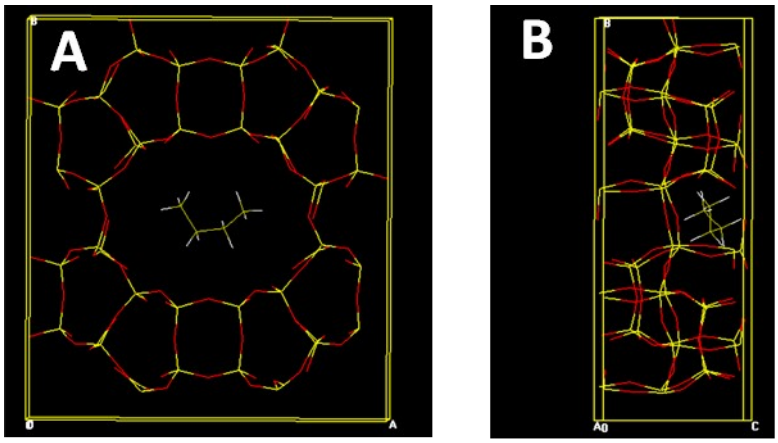

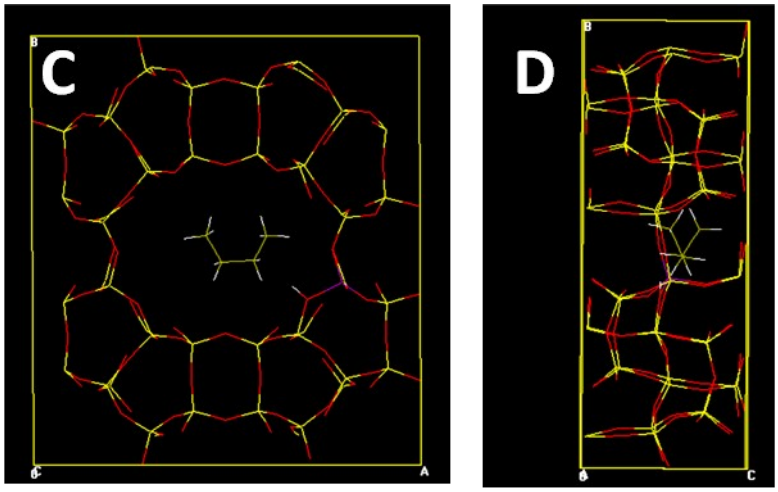

Figure S16: Showing the final calculated geometries of the "g-Butane + Si-MOR DFT" (A-B) and "g-Butane + Al-MOR DFT" (C-D) systems.

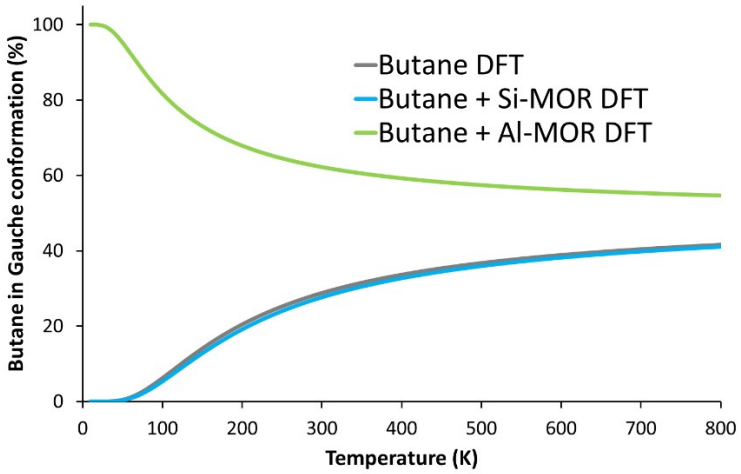

Figure S17: Showing the percentage of n-butane in the gauche conformer as a function of temperature, using a Boltzmann distribution, as a function of temperature, in both unconfined butane (Butane DFT), and butane confined within siliceous mordenite (Butane + Si-MOR DFT) and within acidic Al-substituted mordenite (Butane + Al-MOR DFT)

References

1. S. Brunauer, P. H. Emmett and E. Teller, *Journal of the American Chemical Society*, 1938, **60**, 309-319.
2. E. P. Barrett, L. G. Joyner and P. P. Halenda, *Journal of the American Chemical Society*, 1951, **73**, 373-380.
3. R. S. Pinna, M. Zanetti, S. Rudić, S. F. Parker, J. Armstrong, S. P. Waller, D. Zacek, C. Smith, S. M. Harrison, G. Gorini and F. Fernandez-Alonso, *Journal of Physics: Conference Series*, 2018, **1021**.
4. O. Arnold, J. C. Bilheux, J. M. Borreguero, A. Buts, S. I. Campbell, L. Chapon, M. Doucet, N. Draper, R. Ferraz Leal, M. A. Gigg, V. E. Lynch, A. Markvardsen, D. J. Mikkelson, R. L. Mikkelson, R. Miller, K. Palmen, P. Parker, G. Passos, T. G. Perring, P. F. Peterson, S. Ren, M.

A. Reuter, A. T. Savici, J. W. Taylor, R. J. Taylor, R. Tolchenov, W. Zhou and J. Zikovsky, *Nuclear Instruments and Methods in Physics Research Section A: Accelerators, Spectrometers, Detectors and Associated Equipment*, 2014, **764**, 156-166.
5. R. Dovesi, A. Erba, R. Orlando, C. M. Zicovich-Wilson, B. Civalleri, L. Maschio, M. Rérat, S. Casassa, J. Baima, S. Salustro and B. Kirtman, *Wiley Interdisciplinary Reviews: Computational Molecular Science*, 2018, **8**.
6. S. Grimme, J. Antony, S. Ehrlich and H. Krieg, *J Chem Phys*, 2010, **132**, 154104.
7. S. Grimme, A. Hansen, J. G. Brandenburg and C. Bannwarth, *Chem Rev*, 2016, **116**, 5105-5154.
8. A. D. Becke, *The Journal of Chemical Physics*, 1993, **98**, 5648-5652.
9. C. Lee, W. Yang and R. G. Parr, *Phys Rev B Condens Matter*, 1988, **37**, 785-789.
10. S. H. Vosko, L. Wilk and M. Nusair, *Canadian Journal of Physics*, 1980, **58**, 1200-1211.
11. P. J. Stephens, F. J. Devlin, C. F. Chabalowski and M. J. Frisch, *The Journal of Physical Chemistry*, 2002, **98**, 11623-11627.
12. D. Vilela Oliveira, J. Laun, M. F. Peintinger and T. Bredow, *J Comput Chem*, 2019, **40**, 2364-2376.
13. J. Laun, D. Vilela Oliveira and T. Bredow, *J Comput Chem*, 2018, **39**, 1285-1290.
14. K. Dymkowski, S. F. Parker, F. Fernandez-Alonso and S. Mukhopadhyay, *Physica B: Condensed Matter*, 2018, **551**, 443-448.
15. F. Eder and J. A. Lercher, *Zeolites*, 1997, **18**, 75-81.
16. D. C. Tranca, N. Hansen, J. A. Swisher, B. Smit and F. J. Keil, *The Journal of Physical Chemistry C*, 2012, **116**, 23408-23417.
17. P. Cañizares, A. de Lucas, F. Dorado and D. Pérez, *Applied Catalysis A: General*, 2000, **190**, 233-239.